Discover Quantum Science

RESEARCH Open Access

Quantum information theoretic analysis on the hydrogen atom trapped within a penetrable repulsive barrier potential

Koustav D. Chakladar[1], Santanu Mondal[2], Kalidas Sen[3] and Jayanta K. Saha[1*]

*Correspondence:
Jayanta K. Saha
jksaha.phys@aliah.ac.in
[1]Department of Physics, Aliah University, IIA/27, Newtown, 700160 Kolkata, India
[2]Instituto de Ciencias Físicas, Universidad Nacional Autónoma de Mexico, Av. Universidad S/N, Col. Chamilpa, 62210 Cuernavaca, Morelos, Mexico
[3]School of Chemistry, University of Hyderabad, Hyderabad 500046, India

Abstract

In this study, we aim to investigate the oscillatory nature of the probability density in position and momentum space of a hydrogen atom under a penetrable repulsive single-barrier (RSB) potential and the related information-theoretic measures. We have employed the Ritz variational method, utilizing a Slater-type trial wavefunction to determine the eigenvalues and eigenvectors of the hydrogen atom. The momentum space wavefunction is then estimated by employing the Fourier transformation of the position space counterpart. Both of these conjugate space wavefunctions are used to estimate the Shannon entropy, which is then utilized to verify the well-known Bialynicki-Birula and Mycielski (BBM) inequality. Our investigation reveals confinement-induced oscillatory features in the radial probability density of position space and corresponding oscillations in momentum space. These oscillations are strongly correlated with atomic swelling, orbital fusion, fission, and collapse, which manifest as discontinuities in the variations of the Shannon entropy. For non-zero angular momentum states, additional oscillatory features arise from the combined effect of the centrifugal term and the barrier potential. Altogether, the findings highlight the intricate interplay between external confinement and orbital deformation, their impact on information-theoretic measures, and the consequent emergence of quantum phase transitions.

Keyword Hydrogen atom, Penetrable confinement, Ritz variational method, Shannon entropy, Orbital shape deformation

1 Introduction

Since the pioneering works of Mitchel et al. [1] and Sommerfeld and Welker [2], for nearly 88 years, numerous studies have been conducted on confined atomic and molecular systems for their immense applicability in quantum optics [3], and quantum information theory [4–11]. Due to the enhanced tunability of confining environments, the structural and spectroscopic properties of atoms and molecules can be systematically modified. This, in turn, enables the exploration of various intricate aspects of fundamental physics, such as orbital shape manipulation, including orbital breathing, reordering, fission, and fusion [12]. In this regard, Dolmatov and King [13] investigated the confined

hydrogen atom, focusing on orbital structure manipulation under a finite-barrier potential of the form

$$\mathcal{V}_{\mathrm{RSB}}(r) = \begin{cases} V & R \le r \le R + \Delta, \\ 0 & \text{otherwise} \end{cases} \tag{1}$$

Here V denotes the barrier height, Δ its width, and R the position of the repulsive barrier, respectively. When the hydrogen atom is compressed under this potential and the confinement radius falls below a certain critical value R_c (e.g., $R_c = 1.45$ a.u. for the ground state), the electronic cloud undergoes anomalous swelling, causing the atomic radius to increase to nearly nine times that of the free atom value. The phenomenon, referred to as *atomic swelling*, displays remarkable characteristics, including an abnormal increase in the oscillator strength $f_{1s\to 2p}$, which can become nearly twice the observed value in the corresponding free atom. Similarly, the effect of the finite barrier potential in the many-electron systems has far-fetched implications, where it exhibits phenomena like orbital collapse, orbital fission, and orbital fusion as well. For instance, an excited electron in the 3*d* state of the Chromium atom Cr($3p^5\ 3d^5\ 4s^1\ 3d^*,\ ^7$P), when placed under such a potential, exhibits 3*d* orbital collapse [13]. Another study on such phenomena in the semi-filled states of Phosphorus, Nitrogen, Lithium, and Chromium was carried out by Dolmatov [12]. In another work, Connerade and Dolmatov [14] investigated the controlling orbital-collapse in transition elements using spin-polarized Hartree-Fock wavefunction and particularly demonstrated the controlled orbital collapse in the Cr atom. Also, the finite barrier potential can occur naturally in free *d*- and *f*-block and transition elements, particularly due to the screening effect of the core electrons [15, 16]. Consequently, the Scandide (*d*-block elements) and the Lanthanide (*f*-block elements) contraction arise, resulting in an abrupt reduction of the atomic radius. Interestingly, the structural properties of valence shell electrons in *d*-block and *f*-block elements can be effectively simulated by suitably selecting the parameters $(V,\ R,\ \Delta)$ [17].

When an atom undergoes orbital shape modifications, notable variations in its information-theoretic measures become apparent. In our earlier work [18], we investigated such orbital shape manipulation by studying the changes in the Shannon information entropy for a hydrogen atom. We established that Shannon entropy can be used as an indicator of such orbital shape changes. In that work, the entire calculations were done using the well-established *Lagrange-Laguerre mesh method* (LMM), a simplistic yet highly-accurate numerical technique [19–24]. However, in the case of the finite barrier potential, we have faced few challenges while calculating the potential energy matrix element. Firstly, due to the discontinuous nature of the $\mathcal{V}_{\mathrm{RSB}}(r)$, the chosen Laguerre-type Lagrange functions lose their orthogonality within the range of the potential, and the resulting effect yielded a noticeable numerical instability. However, this can be resolved with proper scaling and transformation of the Lagrange mesh. Secondly, because of the unequal nature of the Gaussian quadrature, the method becomes somewhat problematic for computing the momentum-space density, which is, in fact, an important quantity in the present context. Momentum space density elucidates several properties of an atomic system, such as Compton profiles, atomic form factors *etc*. Despite this, the effect of orbital shape manipulations on the momentum space density of an atomic system and its corresponding information-theoretic measures has not been explored yet.

We note that the information theoretical measures have been previously applied in the analysis of various structural properties in atoms and molecules, for example, in proposing an information theoretical estimate of the exchange parameter of neutral atoms in Xα-theory [25], estimating the mean excitation energy of confined hydrogen atom [26], locating the characteristic minimum in the total Shannon information entropy of the confined atoms [27], analysis of avoided crossing of energy levels of hydrogenic atoms in parallel magnetic and electric fields [28], in the studies involving the chemical bonding in hydrogen molecular ion [29, 30], chemical reactivity description of a three-centre insertion reaction [31], and the characterization of Wigner crystallization [32], respectively. In this work, we present an in-depth investigation of the effects of orbital shape manipulation due to the finite barrier potential on the position as well as the momentum-space density and the subsequent variations in the information-theoretic measures. To avoid the difficulties regarding the calculation of momentum space density, we have used the Ritz variational method by employing the basis set expansion technique instead of LMM. The basis-set expansion technique is a robust method that can be used to solve various types of confined atomic and molecular systems. In fact, various previous works from our group have been done predominantly on the development of the said method [11]. The momentum-space density is calculated using the Fourier transformation of the optimized trial wave-function, which is elaborately pointed out in our previous articles [8, 33]. The Shannon entropy in both position and momentum space is calculated in order to justify the effect of the RSB potential on the hydrogen atom in a more effective way. Additionally, we have also considered the Bialynicki-Birula and Mycielski (BBM) inequality [34] to understand Heisenberg's uncertainty principle in the context of information theory. As an important aspect of this work, various atomic phenomena, such as atomic swelling, orbital fusion, orbital fission, and orbital collapse, have been examined through measuring Shannon entropy for hydrogenic orbitals as functions of the position of the RSB potential. Furthermore, we aim to identify and interpret the discontinuities observed in the Shannon entropy that emerge from sudden structural modifications in the underlying quantum states, thereby signalling the onset of a quantum phase transition.

The article is organized as follows: a brief discussion of the methodology of solving the Schrödinger equation is given in Sec. 2, followed by the discussion on the results in Sec. 3. Lastly, a brief conclusion is presented in Sect. 4.

2 Methodology

The non-relativistic Hamiltonian (in atomic units) of a hydrogen atom under the influence of the repulsive barrier potential (RSB) can be written as [12, 13, 15, 18],

$$\mathcal{H} = -\frac{1}{2}\nabla_r^2 + \mathcal{V}_{\text{eff.}}(r) + \mathcal{V}_{\text{RSB}}(r) \tag{2}$$

where $\hat{\mathcal{T}} = -\frac{1}{2}\nabla_r^2 = -\frac{1}{2}\frac{1}{r^2}\frac{d}{dr}\left(r^2\frac{d}{dr}\right)$ is the radial part of the kinetic energy, $\mathcal{V}_{\text{eff.}}(r)$ is the effective potential which is defined as,

$$\mathcal{V}_{\text{eff.}}(r) = -\frac{1}{r} + \frac{l(l+1)}{2r^2} \tag{3}$$

Here, l is the angular momentum quantum number. To solve Schrödinger's equation for the system, we have employed the Ritz variational method to obtain the variationally optimized energy and position-space wavefunction of the system. Due to the spherical symmetry of the Hamiltonian, we can write the total wavefunction as,

$$\Psi_{nlm}(\mathrm{r}) = \psi_{nl}(r) Y_{lm}(\hat{r}) \tag{4}$$

where $\psi_{nl}(r)$ is the radial wave function and $Y_{lm}(\hat{r})$ represents the spherical harmonics. The explicit expression of $\psi_{nl}(r)$ is considered as the linear combination of a Slater-type basis set, which can be expanded as,

$$\psi_{nl}(r) = r^l \sum_{k}^{N} \mathcal{C}_k \; e^{-\alpha_k r} \tag{5}$$

Here, α_k's are the non-linear variational parameters which are chosen in a geometrical sequence as,

$$\alpha_k = \alpha_{k-1}\sigma \tag{6}$$

Here, σ is the common ratio. The highest and lowest values of α_k along with the value of N are modulated in such a way that the energy eigenvalue of the particular *nl*-state at $V = 0$ becomes accurate up to 14 decimal places. The chosen values of N, α_0, and α_N kept fixed for all calculation of the values of $(V,\ R,\ \Delta)$ at that particular *nl*-state. For example, at 1*s* state, the chosen values are $N = 41$, $\alpha_0 = 0.01$, and $\alpha_N = 500.0$ [8, 10] which remained the same for any further calculations of the 1*s* state itself. The C_k's are known as linear variational parameters, which can be determined by solving the generalized eigenvalue equation, given as,

$$\underline{\underline{\mathcal{H}}}\ \underline{\mathcal{C}} = E\ \underline{\underline{\mathcal{S}}}\ \underline{\mathcal{C}} \tag{7}$$

where $\underline{\underline{\mathcal{H}}}$ is the Hamiltonian matrix, $\underline{\underline{\mathcal{S}}}$ is the overlap matrix, $\underline{\mathcal{C}}$ is the column matrix consisting of linear variational parameters i.e. $\mathcal{C}_k$'s and E is the corresponding energy eigenvalue. We can estimate the radial probability density in the position space as,

$$D_{nl}(r) = r^2 |\psi_{nl}(r)|^2 \tag{8}$$

where,

$$\int_{r=0}^{\infty} D_{nl}(r) dr = 1 \tag{9}$$

The momentum space wave function $\Phi_{nlm}(\mathrm{p})$ can be estimated by performing the 3D Fourier transformation of the position-space wavefunction of Eq. (5)

$$\Phi_{nlm}(\mathrm{p}) = \frac{1}{(2\pi)^{3/2}} \int e^{i\mathrm{p}\cdot\mathrm{r}} \Psi_{nlm}(\mathrm{r}) r^2 dr d\Omega \tag{10}$$

A detailed derivation of the momentum space wavefunction of the Hydrogen atom using the Slater basis is provided in our previous publications of Ref [8, 10, 35]. Now, the expression of the Eq. (10) can be simplified as,

$$\Phi_{nlm}(\mathrm{p}) = \phi_{nl}(p) Y_{lm}(\hat{p}) \tag{11}$$

Here $\phi_{nl}(p)$ and $Y_{lm}(\hat{p})$ are the radial wavefunction and the spherical harmonics in momentum space. The expression of $\phi_{nl}(p)$ can be simplified as,

$$\phi_{nl}(p) = \left[\sqrt{\frac{2}{\pi}} \int_{r=0}^{\infty} i^l j_l(pr)\psi_{nl}(r)r^2 dr\right] \tag{12}$$

Here, $i = \sqrt{-1}$. To proceed further, we need to evaluate the following Fourier-Bessel basis integral,

$$\begin{aligned} \mathcal{A}^q_{l,a}(p) &= \int_{r=0}^{\infty} r^l \; e^{-ar} \; j_q(pr) \; dr \\ &= \sum_{k=0}^{q} \frac{2(q+k)!}{(2p)^{k+1}k!(q-k)!} \frac{(l-k-1)!}{\mathcal{P}_\alpha^{l-k}(p)} \cos\left\{\frac{\pi}{2}(-q+k-1) + (l-k)\xi_\alpha(p)\right\} \end{aligned} \tag{13}$$

where *l* is an integer and must be greater than -1 and $a > 0.0$. Here,

$$\mathcal{P}_\alpha(p) = \sqrt{\alpha^2 + p^2}; \quad \xi_\alpha(p) = \tan^{-1}\left\{\frac{p}{\alpha}\right\} \tag{14}$$

Hence, the expression of $\phi_{nl}(p)$ can be written in terms of $\mathcal{A}^q_{l,a}(p)$ as,

$$\phi_{nl}(p) = \sqrt{\frac{2}{\pi}} i^l \sum_{k}^{N} \mathcal{C}_k \mathcal{A}^l_{l+2,\alpha_k}(p) \tag{15}$$

The radial momentum space density can be written as,

$$\Gamma_{nl}(p) = p^2 |\phi_{nl}(p)|^2 \tag{16}$$

3 Results and discussion

In this section, we have explored the effect of the repulsive barrier potential on the electronic probability densities of the hydrogen atom in the conjugate space. The strength and width of the barrier are fixed at $V = 4.0$ a.u. and $\Delta = 5.0$ a.u. [18], while its position (*R*) is varied to study the resulting changes in the probability densities. Evidently, the atomic swelling in 1*s* state occurs if $V >$2.5 and $\Delta > 1.0$. Thus, the choice of *V* and Δ is sufficient in the present context.

To begin, we evaluated the radial Shannon entropy in both position and momentum space (S_r and S_p), which are defined as:

$$S_r = -\int \rho_{nl}(r) \ln \rho_{nl}(r) r^2 dr; \quad S_p = -\int \gamma_{nl}(p) \ln \gamma_{nl}(p) p^2 dp \tag{17}$$

where, $\rho_{nl}(r) = |\psi_{nl}(r)|^2$, and $\gamma_{nl}(p) = |\phi_{nl}(p)|^2$. The angular Shannon entropy ($S_{\theta,\phi}$) is identical in position and momentum space and can be expressed as:

$$S_{\theta,\phi} = -\int |Y_{lm}(\hat{r})|^2 \ln |Y_{lm}(\hat{r})|^2 d\Omega \; = -\int |Y_{lm}(\hat{p})|^2 \ln |Y_{lm}(\hat{p})|^2 d\Omega \tag{18}$$

The values of $S_{\theta,\phi}$ for different *nl* states are taken from the work of Jiao et al. [36]. Therefore, the total Shannon entropy in position and momentum space (S_r and S_p) can be written as,

$$\mathrm{S}_r = S_r + S_{\theta,\phi}; \quad \mathrm{S}_p = S_p + S_{\theta,\phi} \tag{19}$$

At a specific value of *l*, the $S_{\theta,\phi}$ remains constant in both conjugate position and momentum space due to spherical symmetry. Hence, the value of $S_{\theta,\phi}$ becomes only additive part to S_r and S_p respectively. Now, using the value of S_r and S_p, the Shannon entropy S_T sum can be written as,

$$\mathrm{S}_T = S_r + S_p + 2S_{\theta,\phi} \tag{20}$$

and the corresponding BBM inequality reads as,

$$\mathrm{S}_T \geq 3(1 + \ln \pi) \tag{21}$$

3.1 Zero angular momentum ($l = 0$) states

The effect of the RSB potential has been examined on the conjugate-space radial probability density and the Shannon entropy for the lowest three *s*-symmetric ($l = 0$) states of the hydrogen atom. Prior to this analysis, the wavefunctions of all relevant states were evaluated with high precision, as confirmed by the highly accurate eigenvalues obtained. For instance, at $R = 100.0$ a.u., the energy eigenvalue of the 1*s* state is exactly -0.5 a.u., clearly reflecting the asymptotic free region. Similarly, the eigenvalues for the 2*s* and 3*s* states are found to be -0.125 a.u. and -0.055 a.u., respectively. These results confirm the high accuracy of the computed wavefunctions.

3.1.1 Ground state

At $R = 100$ a.u., the values of S_r and S_p are found to be 4.144 a.u. and 2.422 a.u., respectively, which are consistent (to the digits reported here) with the results of Jiao et al. [36]. Accordingly, the total Shannon entropy S_T at the same *R* is calculated to be 6.567 a.u. As *R* decreases to 2 a.u., S_r reduces to 2.815 a.u., while S_p increases to 3.644 a.u., indicating that the barrier enhances localization of the probability density in position space. In contrast, the probability density in momentum space becomes more delocalized. It is important to note that in both cases, the total Shannon entropy S_T takes the values 6.567 a.u. and 6.459 a.u., respectively, thereby satisfying the BBM inequality. , At $R = 1.45$ a.u., S_r abruptly increases to 10.277 a.u., while S_p decreases to -3.158 a.u. Meanwhile, S_T still maintains the BBM inequality and exhibits a sudden increment up to 7.119 a.u. at same *R*. This sudden change in the information entropy is attributed to atomic swelling [13], and particularly the Shannon entropy can be used as an indicator for such phenomena [18]. These changes also signal the onset of a *quantum phase transition* in the Shannon entropy with respect to the position of the repulsive barrier, *R*. However, to have a better understanding of the underlying intricacies, we need to study the probability densities in both position and momentum space in the utmost detail. For that purpose, we have divided the whole spatial distance into three specific spatial regions: (i) inner attractive region ($0 \leq r \leq R$), (ii) repulsive barrier region ($R < r < R + \Delta$), and (iii) outer attractive region ($R + \Delta \leq r < \infty$). Therefore, the density distribution can be classified into three regions: reflected density (region I), trapped density (region II), and transmitted density (region III). The variations of these radial densities in both position and momentum space are depicted in figure 1 (a) and (b), respectively, for the ground state of the

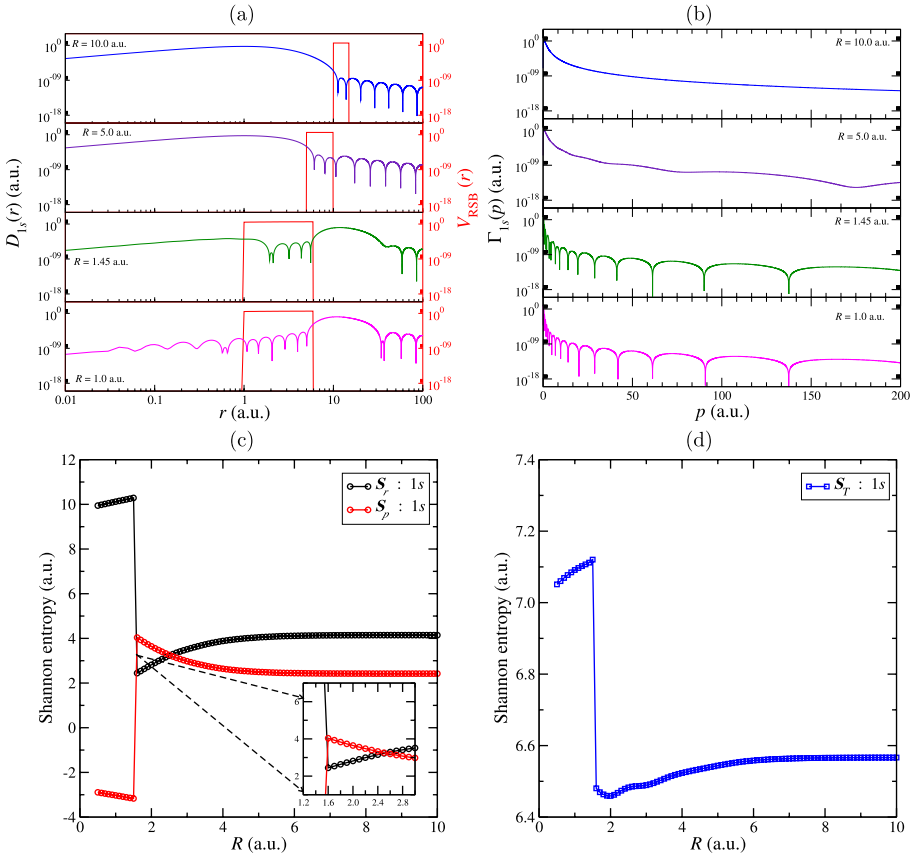

Fig. 1 **a** Position space density and **b** momentum space density of the 1 state of Hydrogen atom for different values of R, **c** Shannon entropy in position space **S** and momentum space **S** and **d** Shannon entropy sum **S** the position of the repulsive single barrier .

hydrogen atom. As evident from figure 1(a), each of these components exhibits distinct patterns when plotted on a logarithmic scale rather than a linear scale.

Before proceeding further, we define two important quantities, such as,

$$\mathcal{D}(a,b) = \int_a^b D(r)dr; \quad \mathcal{G}(a,b) = \int_a^b D(r)\mathcal{V}(r)dr \tag{22}$$

here, $\mathcal{V}(r) = \mathcal{V}_{\text{eff.}}(r) + \mathcal{V}_{\text{RSB}}(r)$. The quantity $\mathcal{D}(a,b)$ indicates the probability of finding the electron within $r \in [a,b]$ while $\mathcal{G}(a,b)$ indicates the strength of the potential within the same region. At $R = 10$ a.u., the quantity $\mathcal{D}(0,R) \equiv \mathcal{D}_{\text{I}}$ (i.e., reflectance for region I) is 0.99999989, indicating that the majority of the electronic cloud is confined within the region $0 \leq r \leq R$, while still retaining nearly all the characteristics of a free atom. The character in the suffix '$\mathtt{I}$' corresponds to the region I, and similar notation is used in the following text. Meanwhile, the value of $\mathcal{D}(R+\Delta,\infty) \equiv \mathcal{D}_{\text{III}}$ (i.e. transmittance) is 1.55×10^{-8}, indicating that the probability of finding the electron in region III is negligibly small. However, despite such a small contribution, the probability distribution in region III has a unique oscillatory feature which can be understood from the quantity $\mathcal{G}(a,b)$. The strength of the potential in the inner well at $R = 10$ a.u. is $\mathcal{G}(0,R) \equiv \mathcal{G}_{\text{I}} = -0.99997874$ a.u., i.e. exactly equivalent to the expectation value of potential energy in the ground state of the hydrogen atom. Due to these reasons, most of the electronic distribution is confined to the region I, maintaining the characteristics

of the free-H atom. In region III, the effect of the potential is almost negligible as $\mathcal{G}(R+\Delta,\infty) \equiv \mathcal{G}_{\rm III} = -7.598 \times 10^{-10}$ a.u. Therefore, in region III, Schrödinger equation can approximately be written as,

$$-\frac{1}{2}\nabla_r^2\psi_{nl}(r) \approx E\psi_{nl}(r) \tag{23}$$

where, $\psi_{nl}(r) \approx j_l(kr)$ with wave vector $k = \sqrt{2E}$. Now, in this limit, the spherical Bessel function attains its asymptotic form $j_l(kr) \approx \frac{\sin(kr - l\frac{\pi}{2})}{kr}$. Therefore, the electronic probability distribution in region III behaves like a free particle with an oscillatory nature. On the other hand, the probability distribution in momentum space shows smooth and monotonic variation with no prospect of oscillation (see figure 1(b)). As the value of R is decreases to 5 a.u., the strength of the inner well ($\mathcal{G}_{\rm I}$) increases to -1.015 a.u. with reflectance ($\mathcal{D}_{\rm I}$) becomes 0.999716. As we can see, due to increased strength in the inner well, the reflected electronic wavefunction in region I becomes localized within a smaller region. This is the compression effect of the finite barrier potential, which is also reflected in the momentum space distribution. From figure 1 (b), it is evident that a small amount of distortion appears in the momentum distribution of the 1s electron. On the other hand, the strength of the outer well increases nearly $\sim 10^4$ times and attains a value of -3.475×10^{-6} a.u. and the value of the transmittance also increases up to $\sim 10^3$ fold ($\mathcal{D}_{\rm III} = 6.151 \times 10^{-5}$). Now, as the value of R further decreases to 1.45 a.u., the strength of the outer well increases to $\mathcal{G}_{\rm III} = -0.079$ a.u., while the value of $\mathcal{G}_{\rm I}$ becomes -3.87×10^{-5} a.u. Due to the increase in the strength of the outer region, the electronic wave tunnels through the repulsive barrier, resulting in atomic swelling, which is evident from the largest lobe of probability density corresponding to the transmitted wave ($\mathcal{D}_{\rm III} = 0.9994878$). Due to this reason, the transmitted part becomes a superposition between 1s-like electronic wavefunction with asymptotic spherical Bessel function of a free particle at a large distance from the nucleus. Interestingly enough, the momentum space distribution of the corresponding swelled hydrogen atom in the ground state exhibits an oscillatory nature, which has only been observed in the case of a one-electron system trapped under an impenetrable cavity. For example, in our earlier work [35], we have elaborately studied the effect of confinement resonance in the momentum space distribution of alkali-like systems under hard-wall confinement. Similarly, we can describe the appearance of the oscillation in momentum space for the swollen hydrogen atom as well. If the strength of the potential barrier is indefinitely increased to infinity in the case of the swollen atom, the resulting potential can be written as,

$$\mathcal{V}_{\rm cage}(r) = \begin{cases} \infty & r < R \\ 0 & \text{Otherwise} \end{cases} \tag{24}$$

Ideally, this is a modified form of the Shell confinement, introduced by Sen [37] with an indefinitely large outer radius. In this particular case, the wavefunction must vanish at the inner radius $r = R$, maintaining the Dirichlet condition. Thus, one may use the trial wavefunction referred in the Ref. [35] to solve the resulting Schrödinger equation using the Ritz variational technique with the spatial limit $r \in [R, \infty)$.

Similarly, the momentum space radial wavefunction can be written as,

$$\phi_{nl}^{\text{cage}}(p) = \left[\sqrt{\frac{2}{\pi}} \int_{r=R}^{\infty} i^l j_l(pr) \psi_{nl}^{\text{cage}}(r) r^2 dr\right] \tag{25}$$

with the Fourier-Bessel basis integral, which can be derived using the expression given in [35],

$$\begin{aligned} \mathcal{A}_{l,a}^{q}(p;R) &= \int_{r=R}^{\infty} r^l \; e^{-ar} \; j_q(pr) \; dr \\ &= \int_{r=0}^{\infty} r^l \; e^{-ar} \; j_q(pr) \; dr - \int_{r=0}^{R} r^l \; e^{-ar} \; j_q(pr) \; dr \end{aligned} \tag{26}$$

$$= e^{-\alpha R} \sum_{k=0}^{q} \sum_{k'=0}^{l} \frac{2(q+k)!(l-k-1)! R^{k'}}{(2p)^{k+1} k! \; k'! (q-k)! \; \mathcal{P}_{\alpha}^{l-k-k'}(p)} \cos\left\{\frac{\pi}{2}(k-q-1) + (l-k-k')\xi_{\alpha}(p) + pR\right\} \tag{27}$$

Now, as it can be seen that due to the presence of pR in the second term of Eq. (26, 27), the momentum space density would exhibit an oscillatory nature. Physically, it can be understood from the fact that due to the attraction of the nucleus, the electron wavefunction would scatter from the inner-hard wall, and the scattered wavefunction will exhibit oscillation that is similar to the case, elaborately pointed out in Ref. [35]. In the present case, this is indeed happening with the swollen hydrogen atom in the presence of the finite barrier, where there exists a non-zero component of the wavefunction inside the region I. For $R = 1$ a.u., an oscillatory pattern appears in the case of the probability density corresponding to the reflected wave (see figure 1(a)). Although the reflectance ($\mathcal{D}_{\text{I}}$) is 5.355×10^{-7}, the oscillation appears since the reflected part of the wave gets trapped within a very small confinement between the nucleus and the repulsive barrier. Meanwhile, the transmitted electronic wave ($\mathcal{D}_{\text{III}} = 0.9994687$) retains its shape similar to $R = 1.45$ a.u., with a slight phase difference due to the change in the value of R.

Now, there exists another interesting and intuitive aspect of this study which was pointed out by Dolmatov et al. [13]. They proposed that within the range of $1.45 \leq R \leq 1.59$ a.u., the strength of inner and outer wells becomes almost comparable, resulting in the emergence of two maxima of $D_{1s}(r)$ in region I and region III, respectively. We have verified this phenomenon, and our calculations indicate that at $R_m = 1.5497$ a.u., the strength of the inner well and outer well becomes almost similar with $\mathcal{G}_{\text{I}} = -0.078$ a.u. and $\mathcal{G}_{\text{III}} = -0.074$ a.u. As predicted by Dolmatov et al. [13], the resulting position space probability distribution in figure 2(a) for $R = 1.5497$ a.u. has two almost comparable maxima for both $D_{1s}(r)$ with $\mathcal{D}_{\text{I}} = 0.048$ and $\mathcal{D}_{\text{III}} = 0.949$. For comparison purposes, we have also depicted the variation of the $D_{1s}(r)$ at $R = 1.45$ a.u. and 1.55 a.u. in figure 2(a) as well. In the case of the former, the reflected part becomes almost negligible as the atom undergoes atomic swelling. For $R = 1.55$ a.u., which is well within the limit of R proposed by Dolmatov et al. [13], there exist two maxima in region I and region III, respectively (see figure 2(a)). In momentum space, however, the momentum space radial wavefunction becomes a superposition of the momentum space counterparts of the reflected and the transmitted wave. The former accounts for the compression-induced distortion, and the latter accounts for the high momentum oscillatory tail. The resulting $\Gamma_{1s}(p)$ for $R = 1.55$ a.u. and $R = 1.5497$ a.u. are depicted in figure 2(b) respectively. The pure oscillatory momentum distribution for the swollen atom in $R = 1.45$ a.u. is also depicted in the figure 2(b).

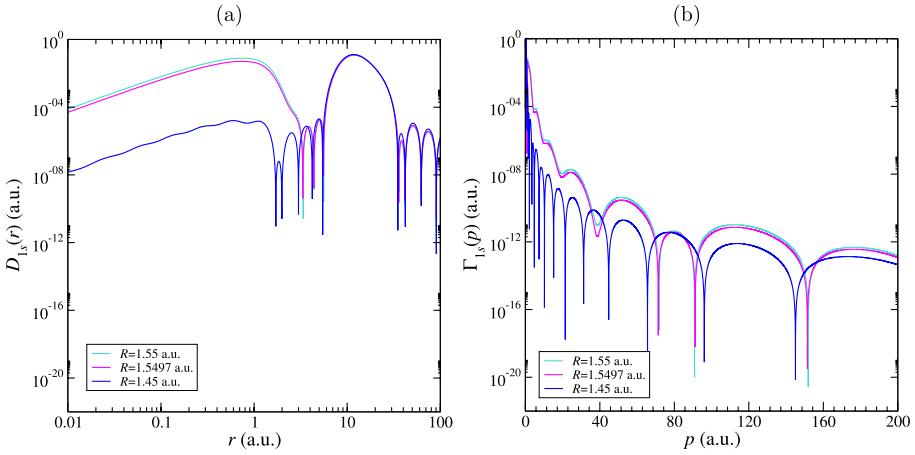

Fig. 2 **a** Position space density $D_{1s}(r)$ and **b** momentum space density $\Gamma_{1s}(p)$ of the 1*s* state of Hydrogen atom for different values of *R* at $R = 1.45,\ 1.5497,\ 1.55$ a.u

3.1.2 Excited states

Next, we have considered a similar discussion on the excited *s*-symmetry states, such as 2*s* and 3*s* states of the hydrogen atom. It is found that as the position of the barrier is shifted closer towards the nucleus, the distribution $D_{2s}(r)$ becomes more localized, and the subsequent momentum space distribution ($\Gamma_{2s}(p)$) becomes more diffused. However, from the variations of S_r, S_p, and S_T with respect to *R*, shown in figure 3(c)-(d), two discontinuities in the Shannon entropy are observed. These correspond to the onset of two significant phenomena: atomic swelling and orbital fusion at $R = 6.4$ a.u., and orbital fission at $R = 1.45$ a.u. [18]. The corresponding variations of the probability densities in conjugate space of the 2*s* state are depicted in the figure 3(a)-(b). At $R = 20$ a.u., the variation of $D_{2s}(r)$ in figure 3(a) in region I shows two distinct lobes, indicating the 2*s*-like electronic distribution. Meanwhile, the transmitted part of the electronic distribution exhibits spherical Bessel-like variation as described earlier. As the value of *R* is decreased to 15 a.u., the distribution $D_{1s}(r)$ in region I becomes more compressed, while the distortions due to the compression effect become prominent in the variation of $\Gamma_{2s}(p)$. Now, the atomic swelling of 2*s* state and the subsequent orbital fusion occur at $R = 6.4$ a.u. compared to $R = 6.48$ a.u. [18]. The orbital fusion occurs when the two distinct lobes of the position probability density of 2*s* electronic state merge together to form a 1*s*-like feature, which is generally accompanied by the atomic swelling. The corresponding momentum distribution at $R = 6.4$ a.u. shows oscillatory features. Similarly, the orbital fission in 2*s* state occurs exactly at $R = 1.45$ a.u., which happens to be the value of *R* at which the atomic swelling occurs in 1*s* state. This trend continues for all excited states as well. Also, the momentum space distribution at $R = 1.45$ a.u. retains its oscillatory features with a small phase shift due to the position of the barrier. Similar to the 1*s* state, at $R_m = 1.51291$ a.u., the strength of the inner well ($\mathcal{G}_{\mathrm{I}} = -0.044$ a.u.) and outer well ($\mathcal{G}_{\mathrm{III}} = -0.046$ a.u.) becomes comparable.

However, for the 3*s* state, four distinct discontinuities appear in the variations of the Shannon entropy, as shown in figure 4(c)–(d). These correspond to atomic swelling and orbital fusion at $R = 14.3$ a.u., orbital collapse and the first orbital fission at $R = 6.4$ a.u., a second atomic swelling at $R = 5.5$ a.u., and a second orbital fission at $R = 1.45$ a.u. The first phenomenon is very similar to the cases which are described for the 1*s* and

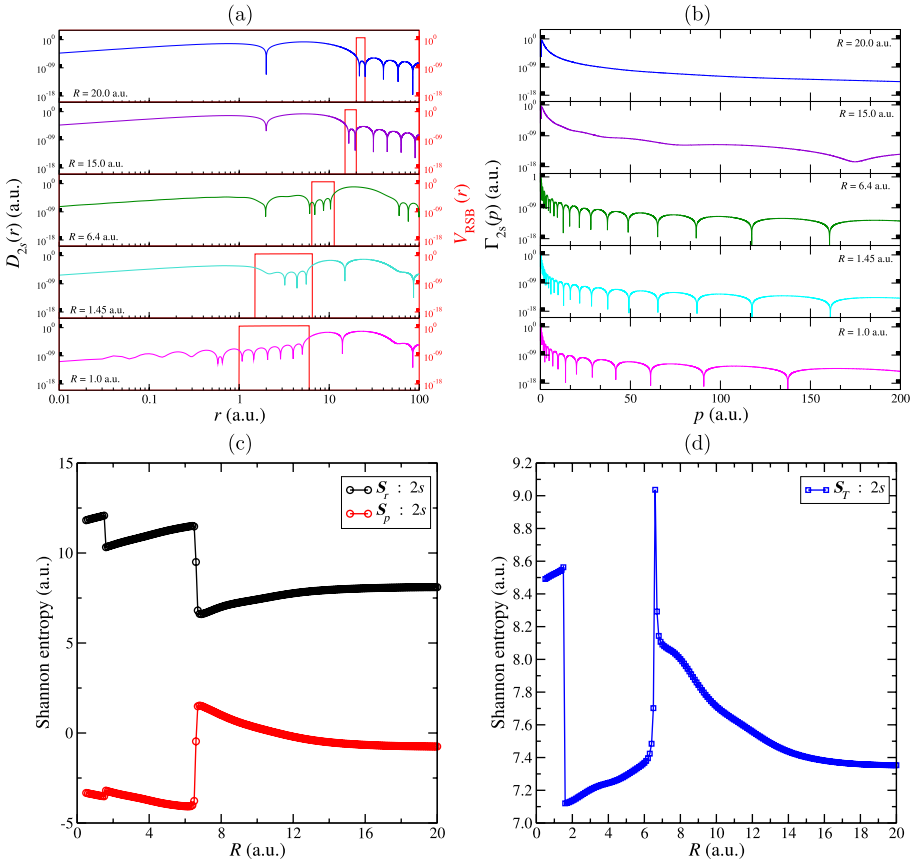

Fig. 3 **a** Position space density $D_{2s}(r)$ and **b** momentum space density $\Gamma_{2s}(p)$ of the 2*s* state of Hydrogen atom for different values of *R*, **c** Shannon entropy in position space S_r and momentum space S_p and **d** Shannon entropy sum S_T *w.r.t.* the position of the repulsive single barrier *R*

2*s* states, respectively. At $R = 14.3$ a.u., the three distinct lobes of the $D_{3s}(r)$ merged to form 1*s*-like distribution, as evident from the figure 4 (a). The resulting momentum space density exhibits oscillatory features as well (see figure 4(b)). However, the orbital collapse, or sudden compression, occurs when the entire transmitted electronic wave from region III tunnels back into region I ($\mathcal{D}_{\rm I} = 0.979$). This is caused by the abrupt increase in the strength of the inner well ($\mathcal{G}_{\rm I} = -0.442$ a.u.) relative to the outer well ($\mathcal{G}_{\rm III} = -0.0006$ a.u.). Additionally, the probability distribution in region I contains two distinct lobes, similar to the 2*s* state, indicating the occurrence of the first orbital fission. A small yet non-negligible portion of the transmitted wave can also be found as $\mathcal{D}_{\rm I} = 0.016$, which has a profound implication on the momentum space density. Now, due to this reason, the $\Gamma_{3s}(p)$ becomes a superposition of the momentum space counterpart of both reflected as well as transmitted waves, resulting in a momentum distribution that has a compression-induced distortion and oscillation (see figure 4(b)). Now, as the value of *R* is decreased even further from $R = 6.4$ a.u. to $R = 5.5$ a.u., due to the compression effect, the electronic cloud tunnels back to the region III, maintaining its 2*s*-like feature (see figure 4(a)). Therefore, it can be considered as the 2nd atomic swelling, which is also the reason behind the sharp rise in the value of S_r near $R = 5.5$ a.u. The corresponding $\Gamma_{3s}(p)$ exhibits the oscillatory features similar to the first atomic swelling with a small phase shift as well (see figure 4(a)). At $R = 1.45$ a.u., the second orbital fission occurs. Due to this reason, the variation of $D_{3s}(r)$ in region III contains the three

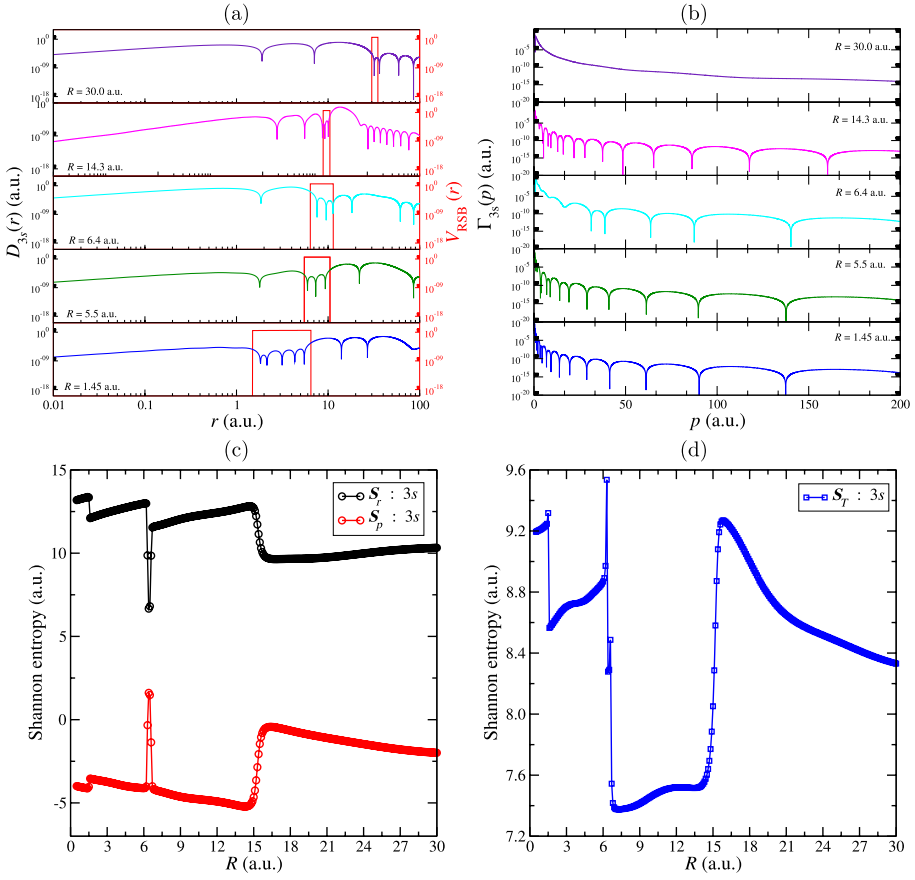

Fig. 4 **a** Position space density $D_{3s}(r)$ and **b** momentum space density $\Gamma_{3s}(p)$ of the 3*s* state of Hydrogen atom for different values of *R*, **c** Shannon entropy in position space S_r and momentum space S_p and **d** Shannon entropy sum S_T *w.r.t.* the position of the repulsive single barrier (*R*)

distinct lobes. The corresponding $\Gamma_{3s}(p)$ shows no distinct changes in the oscillation. It is also observed that, between $R = 1.5$ a.u. and $R = 1.5001$ a.u., the strength of the inner well ($\mathcal{G}_{\rm I}$) decreases drastically relative to the outer well ($\mathcal{G}_{\rm III}$), suggesting that within this narrow range there exists a value of *R* at which the strengths of the inner and outer wells become comparable. However, it should be mentioned that for higher excited states i.e. 3*s*, 4*s*, and so on, the precise estimation of the value of R_m becomes extremely difficult and notoriously sensitive.

3.2 Non-zero angular momentum ($l \neq 0$) states

For $l \neq 0$ states, such as 2*p*, 3*p*, and 3*d*, the presence of the centrifugal term in the Hamiltonian behaves as an additional repulsive barrier for region I. Thus, it can be thought that the resulting electronic wavefunction gets trapped within two repulsive barriers. Due to this reason, the amplified effect of compression can generate oscillation within the momentum space density before the atomic swelling. For example, at $R = 15$ a.u., the variation of $D_{2p}(r)$ in figure 5(a) shows that the electronic cloud becomes compressed within two repulsive barriers. The corresponding momentum distribution of $\Gamma_{2p}(p)$ shows the oscillatory nature in the high momentum range (see figure 5(b)) that is absent in the *s*-symmetry states, which is discussed earlier. Further, as *R* decreases to $R = 5.3$ a.u., the atomic swelling occurs in the 2*p* state of the system, and the resulting

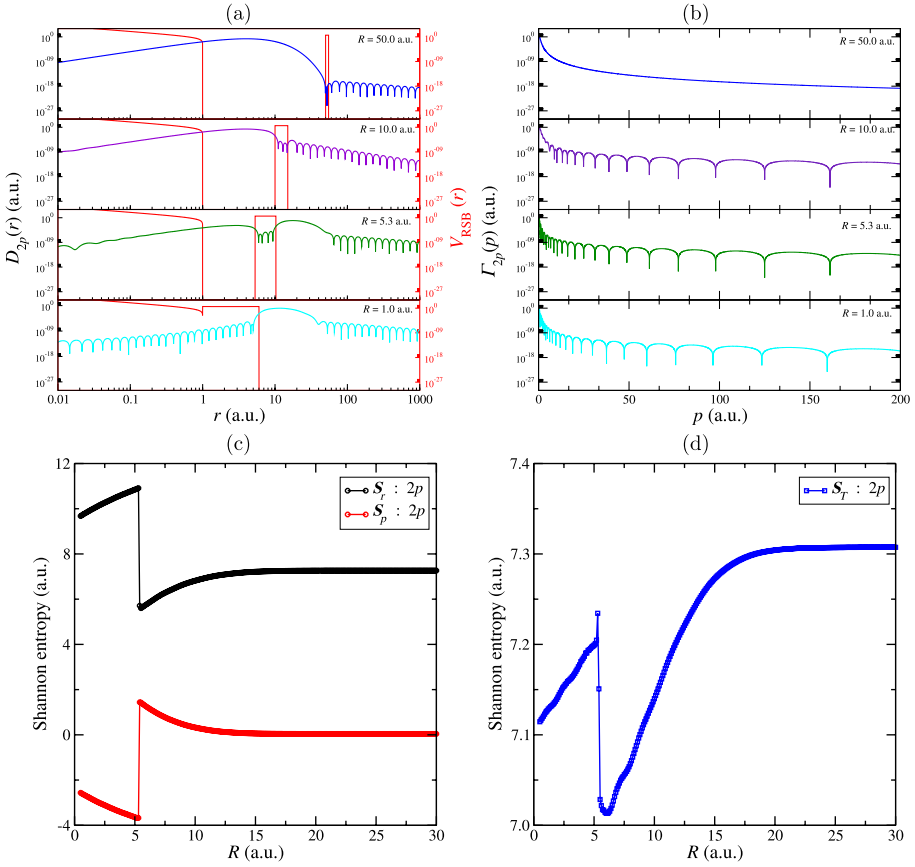

Fig. 5 **a** Position space density $D_{2p}(r)$ and **b** momentum space density $\Gamma_{2p}(p)$ of the $2p$ state of Hydrogen atom for different values of R, **c** Shannon entropy in position space S_r and momentum space S_p and **d** Shannon entropy sum S_T *w.r.t.* the position of the repulsive single barrier R

distribution of $D_{2p}(r)$ exhibits the presence of a larger singular lobe in region III. Contrary to $R = 15$ a.u., the oscillation in $\Gamma_{2p}(p)$ at $R = 5.3$a.u. can be seen in the low momentum range as well. At $R = 1$ a.u., however, the two repulsive barriers merge together to form a single repulsive barrier, which extends all throughout the region I. Interestingly, the portion of the electronic wave that gets trapped within the repulsive barrier also exhibits oscillatory behavior in the position space distribution. Although it is prevalent for all the cases described earlier (i.e. the region II), the oscillation in $D_{nl}(r)$ inside the repulsive barrier becomes more prominent for $l \neq 0$ state around $R \sim 1$ a.u. Similarly, for the $3d$ state, oscillations in the high-momentum region of the distribution $\Gamma_{3d}(p)$ are observed due to the compression effect at $R = 15$ a.u. (see figure 7(b)), while atomic swelling occurs at $R = 11.4$ a.u. In cases of both $2p$ and $3d$ states, the variation of the Shannon entropy exhibits a singular discontinuity in its variation *w.r.t.* R (see figure 5(c)-(d) and 7(c)-(d)) [18].

For the $3p$ state, the variation of the Shannon entropy exhibits three distinct discontinuities (see figure 6(c)–(d)): atomic swelling and orbital fusion near $R = 13.6$ a.u., sudden compression or orbital collapse at $R = 5.3$ a.u., and orbital fission accompanied by a second atomic swelling at $R = 5.0$ a.u. The corresponding variations of $D_{3p}(r)$ and $\Gamma_{3p}(p)$ are demonstrated in figure 6(a)-(b), respectively. From the figure 6 (a), the usual atomic swelling and the subsequent orbital fusion can be evident by seeing the presence of a singular $2p$-like lobe in the region III of the distribution of $D_{3p}(r)$. The resulting

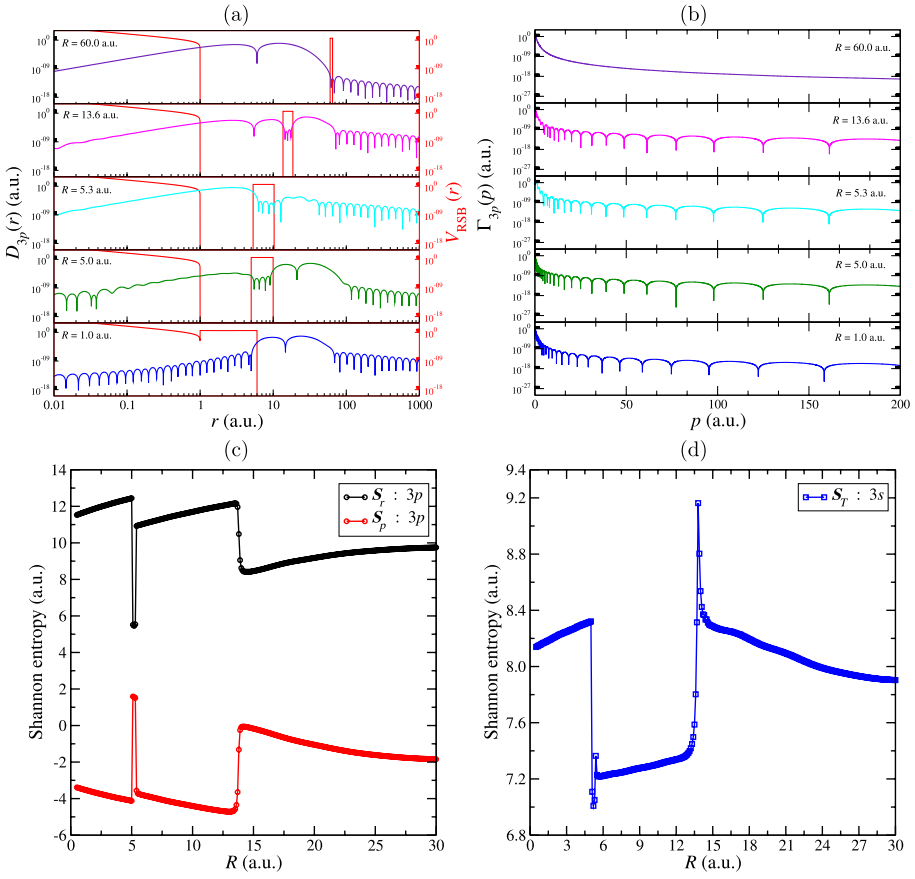

Fig. 6 **a** Position space density $D_{3p}(r)$ and **b** momentum space density $\Gamma_{3p}(p)$ of the 3*p* state of Hydrogen atom for different values of *R*, **c** Shannon entropy in position space S_r and momentum space S_p and **d** Shannon entropy sum S_T *w.r.t.* the position of the repulsive single barrier *R*

$\Gamma_{3p}(p)$ shows the presence of the oscillation as well. However, near $R = 5.3$ a.u., the strength of the inner well increases to ($\mathcal{G}_{\rm I} = -0.204$ a.u.), which is almost $\sim 10^5$ times higher than the strength of the outer well ($\mathcal{G}_{\rm III} = -8.307 \times 10^{-5}$ a.u.), resulting in the orbital collapse. Due to this reason, the entire electronic cloud tunnels back to region I from region III, which is also depicted from the variation of $\Gamma_{3p}(p)$. When the value of *R* is further reduced to $R = 5$ a.u., the electronic cloud exhibits another atomic swelling similar to 3*s* state, and it is also accompanied by orbital fission.

Finally, a summary of all the phenomena observed for different states of the hydrogen atom under consideration is provided in Table 1 for further clarification. Interestingly, all of these orbital shape manipulations, listed in the second column in Table 1, can be construed as QPT, which is fundamentally different from the classical thermal phase transition process. While the latter is driven by thermal fluctuations, a QPT can be induced by varying a non-thermal parameter (NPT) in the system's Hamiltonian [38]. When such a parameter reaches a critical value, the ground state of the quantum system undergoes a fundamental change, signalling the onset of QPT [39]. In a seminal work, Serra and Kais [40] demonstrated a profound connection between electronic structure theory and quantum critical phenomena. They showed that the symmetry breaking of an electronic configuration *w.r.t* a particular NTP is an essential feature of a quantum phase transition. Within this framework, parameters such as the nuclear charge of an atom or the inverse

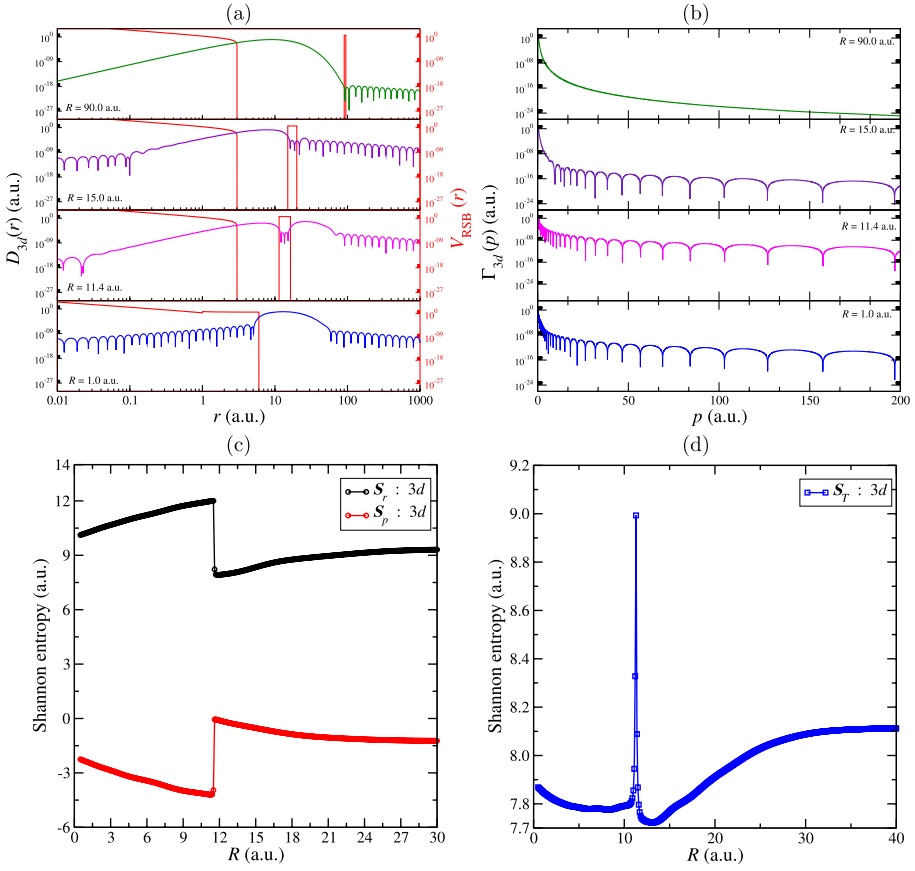

Fig. 7 **a** Position space density $D_{3d}(r)$ and **b** momentum space density $\Gamma_{3d}(p)$ of the 3*d* state of Hydrogen atom for different values of *R*, **c** Shannon entropy in position space S_r and momentum space S_p and **d** Shannon entropy sum S_T *w.r.t.* the position of the repulsive single barrier *R*

Table 1 The specific values of the position of the barrier, *R* (in a.u.), at which different types of orbital shape deformation occur for the trapped hydrogen atom

States	Atomic phenomenon	*R*
1*s*	Swelling	1.45
2*s*	Swelling and orbital fusion	6.40
	Orbital fission	1.45
2*p*	Swelling	5.30
3*s*	Swelling and orbital fusion	14.30
	Orbital collapse and fission	6.40
	Second swelling	5.50
	Second orbital fission	1.45
3*p*	Swelling and orbital fusion	13.60
	Orbital collapse	5.30
	Orbital fission with swelling	5.00
3*d*	Swelling	11.40

internuclear distance in molecules play a role analogous to that of temperature in classical phase transitions. Subsequent research has established that two-electron systems bound via the Coulomb interaction undergo such a QPT in the vicinity of critical charge, where a symmetry breaking occurs in the two-particle density. Furthermore, some studies revealed properties like radial and angular momenta exhibit abrupt changes near critical points [41–47]. In view of this, the present work shows several sharp changes are

noted in the Shannon entropy profile, indicating the orbital nodal structure manipulation with the change of the NTP of the Hamiltonian, that is, the position of the barrier *R*. For the ground state, the system undergoes a transition from a low polarizability state to a swollen high polarizability state. So, one can opine that the Shannon entropy profile, being an explicit function of the orbital density, indicates the quantum phase transition for the confined system under the present consideration.

4 Conclusion

In the present work, we investigate the influence of a penetrable repulsive single-barrier (RSB) potential on orbital shape manipulation of *nl* states ($n = 1 - 3$ and $l = 0 - 2$) of the hydrogen atom. Specifically, we analyze phenomena such as orbital breathing, reordering, fission, and fusion under the effect of this potential. In our earlier study [18], these processes were systematically examined to provide a comprehensive understanding of the hydrogen atom, where Shannon entropy was shown to serve as an effective indicator of orbital shape manipulation. In that study, the Schrödinger equation was solved using the Lagrange mesh method (LMM) with the aid of a high-accuracy Gauss–Laguerre mesh. However, certain challenges were encountered, primarily due to the discontinuous nature of the RSB potential and the non-uniform characteristics of the Gaussian quadrature. These issues are well taken care of by introducing here the Ritz variational method with the help of a Slater-type basis set. The variationally optimized wave function is then used to determine the momentum space wave function with the help of the Fourier transformation of the position space counterpart. First, we evaluate the position- and momentum-space Shannon entropies for various parameters of the RSB potential, namely the height (V_0), width (Δ), and position (R). To gain deeper insight, the whole configuration space is divided into three distinct regions: the inner attractive region ($r \leq R$), the repulsive barrier region ($R < r < R + \Delta$), and the outer attractive region ($r \geq R + \Delta$). The analysis of Shannon entropy in both position and momentum space reveals that the system exhibits increased localization as R decreases, while simultaneously supporting the phenomena mentioned above. A number of discontinuities, depending on both n and l, are observed in the variations of the Shannon entropy in position and momentum space. These discontinuities mark the onset of a quantum phase transition. In the present work, however, we do not explore the details of this transition; instead, we treat it simply as a sudden modification, leaving a more comprehensive analysis for future studies. The Shannon entropy in the conjugate spaces is further employed to analyze the origin of these discontinuities, thereby distinguishing whether they arise from atomic swelling, atomic collapse, or orbital fusion and fission. Furthermore, the Bialynicki-Birula and Mycielski (BBM) entropic uncertainty relation is examined and found to hold consistently for the entire spatial domain. Next, the probability density is used to estimate the reflectance, transmittance, and absorptance for the three different regions mentioned above. It is observed that for R sufficiently high, for the ground state of hydrogen atom, the probability distribution is predominantly concentrated within the inner region, yielding a reflectance value close to unity, while transmission remains negligible. Nevertheless, the probability density exhibits oscillatory behavior, arising from the interaction of the hydrogen atom with the potential well. Interestingly, such oscillations are absent in the momentum-space density distribution. Moreover, a reduction in R leads to an increasingly localized wave function,

whereas beyond a certain critical value of R, the system undergoes atomic swelling and the momentum space distribution demonstrates oscillation. For the ground state of the hydrogen atom, we find that at $R = R_m \approx 1.5497$ a.u., the density distribution exhibits comparable peak amplitudes in the first and third regions, indicating an equivalent contribution from the inner well and the outer well of the potential. A similar characteristic is observed for all the other excited states considered, although the corresponding value of R_m varies from state to state. Additionally, we observe that different states exhibit different numbers of atomic phenomena, with their specific positions also identified. Overall, the present calculations demonstrate the effectiveness of the employed methodology, as well as the utility of Shannon entropy, in capturing and elucidating various fundamental physical phenomena through the orbital shape analysis of different states of the hydrogen atom confined within the RSB potential.

Author contributions
Koustav D. Chakladar: Code development, Data curation, Visualization, Writing–original draft; Santanu Mondal: Writing and reviewing the draft; Kalidas Sen: Writing and reviewing the draft; Jayanta K. Saha: Conceptualisation, Method, Investigation, Data validation, Writing and reviewing the draft, Funding acquisition

Funding
JKS acknowledges partial financial support from the Anusandhan National Research Foundation (ANRF) [erstwhile Science and Engineering Research Board (SERB)], Govt. of India, under file number CRG/2022/003547 and Aliah University Research and Development Cell (AURDC) under file number AURDC/2024-25/PHY/02.
The postdoctoral stay of the SM is supported by the DGAPA-UNAM Postdoctoral Scholarship Program.
KDS thanks the Indian National Science Academy, New Delhi, for the grant INSA/SP/SS/2023 under the Honorary Scientist program.

Data availability
All data that support the findings of this study are included within the article (and any supplementary files).

Declarations

Ethics approval and consent to participate
Not Applicable.

Consent for publishcation
Not Applicable.

Competing interests
The authors declare no Conflict of interest.

Received: 16 September 2025 / Revised: 3 December 2025 / Accepted: 9 December 2025
Published online: 17 February 2026

References

1. Michels A, De Boer J, Bijl A. Remarks concerning molecural interaction and their influence on the polarisability. Physica. 1937;4:981. https://doi.org/10.1016/S0031-8914(37)80196-2.
2. Sommerfeld A, Welker H. Künstliche Grenzbedingungen beim Keplerproblem. Annalen der Physik. 1938;424:56. https://doi.org/10.1002/andp.19384240109.
3. Ducloy M, Bloch D. Quantum optics of confined systems, Vol. 314 (Springer Dordrecht, 1996) https://doi.org/10.1007/978-94-009-1657-9
4. Lin Y-C, Fang T-K, Ho YK. Quantum entanglement for helium atom in the Debye plasmas. Phys Plasmas. 2015;22:032113. https://doi.org/10.1063/1.4916064.
5. Kościk P, Saha JK. Entanglement in helium atom confined in an impenetrable cavity. Eur Phys J D. 2015;69:1. https://doi.org/10.1140/epjd/e2015-60453-4.
6. Mondal S, Nayek SK, Saha JK. Ground and doubly excited states of He atom in non-ideal classical plasmas: structural, entanglement and information theoretical measures. Eur Phys J Plus. 2022;137:373. https://doi.org/10.1140/epjp/s13360-022-02574-1.
7. Mondal S, Sen K, Saha JK. He atom in a quantum dot: structural, entanglement, and information-theoretical measures. Phys Rev A. 2022;105:032821. https://doi.org/10.1103/PhysRevA.105.032821.
8. Mondal S, Sadhukhan A, Sen KD, Saha JK. Structural properties and quantum information measures of H, Li and Na atoms endohedrally captured in C and C cages. Eur Phys J Plus. 2023;138:576.https://doi.org/10.1088/1361-6455/ace177
9. Mondal S, Sadhukhan A, Sen K, Saha JK. Journal of Physics B: Atomic. Mol Optical Phys. 2023;56:155001. https://doi.org/10.1088/1361-6455/ace177.
10. Mondal S, Sadhukhan A, Saha JK, Roy AK. Journal of Physics B: Atomic. Mol Opt Phys. 2024;57:175001. https://doi.org/10.1088/1361-6455/ad5fd3.

11. Chakladar KD, Mondal S, Sen K, Saha JK. Quantum-information-theoretic analysis of Zee systems under pressure confinement. Phys Rev A. 2024;110:042819. https://doi.org/10.1103/PhysRevA.110.042819.
12. Dolmatov VK. Journal of Physics B: Atomic. Mol Optical Phys. 2013;46:095005. https://doi.org/10.1088/0953-4075/46/9/095005.
13. Dolmatov V, King J. Journal of Physics B: Atomic. Mol Optical Phys. 2012;45:225003. https://doi.org/10.1088/0953-4075/45/22/225003
14. Connerade JP, Dolmatov VK. Journal of Physics B: Atomic. Mol Optical Phys. 1998;31:3557. https://doi.org/10.1088/0953-4075/31/16/009.
15. Connerade JP, Dolmatov VK, Lakshmi PA. The filling of shells in compressed atoms. J Phys At Mol Opt Phys. 2000;33:251. https://doi.org/10.1088/0953-4075/33/2/310.
16. Connerade J-P. Confining and compressing the atom. Eur Phys J D. 2020;74:1.https://doi.org/10.1140/epjd/e2020-10414-y
17. Connerade J, Dolmatov V, Lakshmi PA. Journal of Physics B: Atomic. Mol Opt Phys. 2000;33:251.class="oxeins_1" id="oxe_insert_1_1766172168725_9380382063914359" user="Jayanta K. Saha" insertedat="12-19-2025 11:22:48"> https://doi.org/10.1088/0953-4075/33/2/310
18. Das Chakladar K, Mondal S, Bhattacharyya S. Shannon entropy as an indicator for the orbital shape manipulation of a hydrogen atom under a repulsive single barrier potential. Suplemento de la Revista Mexicana de Física. 2025;6:1–9, 011305. https://doi.org/10.31349/SuplRevMexFis.6.011305.
19. Baye D, Heenen P-H. Generalised meshes for quantum mechanical problems. J Phys Math Gen. 1986;19:2041.https://doi.org/10.1088/0305-4470/19/11/013
20. Baye D. Journal of Physics B: Atomic. Mol Opt Phys. 1995;28:4399. https://doi.org/10.1088/0953-4075/28/20/005
21. Baye D, Hesse M, Vincke M. The unexplained accuracy of the Lagrange-mesh method. Phys Rev E. 2002;65:026701. class="oxeins_1" id="oxe_insert_1_1766171700388_2791210587775621" user="Jayanta K. Saha" insertedat="12-19-2025 11:15:00"> https://doi.org/10.1103/PhysRevE.65.026701
22. Baye D, Sen KD. Confined hydrogen atom by the Lagrange-mesh method: energies, mean radii, and dynamic polarizabilities. Phys Rev E. 2008;78:026701. https://doi.org/10.1103/PhysRevE.78.026701.
23. Baye D. the Lagrange-mesh method. Phys Rep. 2015;565:1. https://doi.org/10.1016/j.physrep.2014.11.006.
24. Baye D, Dohet-Eraly J. Confined helium on Lagrange meshes. Phys Chem Chem Phys. 2015;17:31417. https://doi.org/10.1039/C5CP00110B
25. Raju K, Nair P, Sen K. An information-theoretical estimate of the exchange parameter in Xα theory. Chem Phys Lett. 1990;170:89. https://doi.org/10.1016/0009-2614(90)87094-8.
26. Banerjee A, Sen K, Garza J, Vargas R. Mean excitation energy, static polarizability, and hyperpolarizability of the spherically confined hydrogen atom. J Chem Phys. 2002;116:4054. https://doi.org/10.1063/1.1449460
27. Sen KD. Characteristic features of Shannon information entropy of confined atoms. J Chem Phys. 2005;123:074110. https://doi.org/10.1063/1.2008212.
28. González-Férez R, Dehesa J, Patil S, Sen K. Scaling properties of composite information measures and shape complexity for hydrogenic atoms in parallel magnetic and electric fields. Phys A. 2009;388:4919.https://doi.org/10.1016/j.physa.2009.08.007
29. Montgomery H, Sen K. Statistical complexity and Fisher–Shannon information measure of H_2^+. Phys Lett A. 2008;372:2271. https://doi.org/10.1016/j.physleta.2007.11.041.
30. Montgomery H, Sen K. Physics Letters A. 2017;381:2557. https://doi.org/10.1016/j.physleta.2017.05.062.
31. Esquivel RO, Flores-Gallegos N, Dehesa JS, Angulo JC, Antolín J, López-Rosa S, et al. Phenomenological description of a three-center insertion reaction: an information-theoretic study. J Phys Chem A. 2010;114:1906. https://doi.org/10.1021/jp908898w.
32. Thompson DC, Anderson JSM, Sen KD. Information theory and wigner crystallization: a model perspective. Int J Quantum Chem. 2021;121:e26549. https://doi.org/10.1002/qua.26549.
33. Mondal S, Saha JK, Mukherjee PK, Fricke B. Information theoretic measures on the two-photon transitions of hydrogen atom embedded in weakly coupled plasma environment. Phys Script. 2023;98:045411. https://doi.org/10.1088/1402-4896/acc2f2.
34. Białynicki-Birula I, Mycielski J. Uncertainty relations for information entropy in wave mechanics. Commun Math Phys. 1975;44:129. https://doi.org/10.1007/BF01608825.
35. Chakladar KD, Mondal S, Bhattacharyya S, Sen K, Saha JK. Journal of Physics B: Atomic. Mol Opt Phys. 2025;58:075003. https://doi.org/10.1088/1361-6455/adc525.
36. Jiao LG, Zan LR, Zhang YZ, Ho YK. Benchmark values of Shannon entropy for spherically confined hydrogen atom. Int J Quan Chem. 2017;117:e25375. https://doi.org/10.1002/qua.25375.
37. Sen KD. The Journal of Chemical Physics. J Chem Phys. 2005;122:194324. https://doi.org/10.1063/1.1901584.
38. Roch N, Florens S, Bouchiat V, Wernsdorfer W, Balestro F. Quantum phase transition in a single-molecule quantum dot. Nature. 2008;453:633. https://doi.org/10.1038/nature06930.
39. Sondhi SL, Girvin SM, Carini JP, Shahar D. Continuous quantum phase transitions. Rev Mod Phys. 1997;69:315. https://doi.org/10.1103/RevModPhys.69.315.
40. Serra P, Kais S. Critical phenomena for electronic structure at the large-dimension limit. Phys Rev Lett. 1996;77:466. https://doi.org/10.1103/PhysRevLett.77.466.
41. Islam R, Edwards E, Kim K. Onset of a quantum phase transition with a trapped ion quantum simulator. Nature Commun. 2011;2:377. https://doi.org/10.1038/ncomms1374.
42. S H, van der Zant J, Fritschy FC, Elion WJ, Geerligs LJ, Mooij JE. Phys. Rev. Lett. 1992;69:2971 https://doi.org/10.1103/PhysRevLett.69.2971
43. Osterloh A, Amico L, Falci G, Fazi R. Scaling of entanglement close to a quantum phase transition. Nature. 2002;416:608. https://doi.org/10.1038/416608a.
44. Pawlak, Mariusz and Mondal, Santanu and Sadhukhan, Anjan and Sen, Kalidas and Saha, Jayanta K. International Journal of Quantum Chemistry 2025;125: e70042 https://doi.org/10.1002/qua.70042
45. Sadhukhan, Anjan and Dutta, Sayantan and Saha, Jayanta K. International Journal of Quantum Chemistry 2019;119:e26042 https://doi.org/10.1002/qua.26042

46. Gu S-J, Lin H-Q, Li Y-Q. Entanglement, quantum phase transition, and scaling in the XYZ chain. Phys Rev A. 2003;68:042330. https://doi.org/10.1103/PhysRevA.68.042330.
47. Vidal J, Palacios G, Mosseri R. Entanglement in a second-order quantum phase transition. Phys Rev A. 2004;69:022107. https://doi.org/10.1103/PhysRevA.69.022107.